

DEVELOPMENT OF FATIGUE FAILURE CRITERIA
FOR DARLINGTON FUEL BUNDLE ENDPLATES

E.T.C. Ho, G.K. Shek, M.L. Vanderglas & M. Leger
Ontario Hydro Research Division
800 Kipling Ave, Toronto, Ontario

ABSTRACT

The fatigue limits of the endplate-to-endcap welds of the Ontario Hydro 37 element fuel bundle were established by testing small specimens. The results indicated an effective stress concentration factor of four due to the weld geometry. Higher mean stress reduced the fatigue limit in samples which failed in one million cycles. For tests carried out at high R-ratio, a stress amplitude of 45 MPa produced failures between 10^5 and 10^6 cycles. The fractographic features of the Darlington fuel bundle endplate cracks are consistent with the features of the low stress high cycle fatigue cracks produced in the small specimen test program.

1.0 INTRODUCTION

Refuelling problems encountered on channel N12 of Darlington Unit 2 were caused by loss of fuel bundle integrity resulting from cracks in the endplate. Subsequent examination showed that cracks were also found in fuel bundles located in some other channels in columns 12 and 13. Most of the cracks were associated with the endplate-to-endcap welds. Fatigue was initially proposed as the likely mechanism of cracking and this was confirmed by subsequent fractography. Fatigue life data were required for failure analysis to identify the possible source and magnitude of the cyclic stresses to induce failure. Initial assessment of fatigue life performed by the fuel bundle manufacturer was based on literature fatigue data for Zircaloy-2(1) and an assumed stress concentration factor for the weld geometry. This paper describes a test program using small specimen to simulate the failed component to obtain fatigue life data for the endplate-to-endcap welds. In addition, the small specimens were also used to study specific fatigue fracture features which are relevant to the failure investigation. Some of the fatigue cracks from the small specimen program were characterized by fractography and metallography for comparison with cracks from the field failures in order to determine the conditions of cracking.

The small specimen program to obtain fatigue life data was implemented early on in the failure investigation when the best information on the cracks was the video inspection of the downstream endplate of the outlet bundle in channel K12 (Figure 1). During initial discussion regarding modes of loading which could produce such cracks, it was generally agreed that

time-varying hydraulic drag forces in the bundle axial direction appeared to be a good possibility. The small specimen program was designed to satisfy two main criteria: first, that the specimen adequately simulate the failed component; and second, that the stress analysis of the specimen would be straight forward. The specimen was designed to simulate the loading on pencils on the outer ring which were not supported by the latch.

2.0 EXPERIMENTAL

The design of the endplate-to-endcap weld specimens for fatigue evaluation is shown in Figure 2. The width of the endplate strip and the spacing between endcaps were selected to correspond to those of the outer ring of a standard Ontario Hydro 37-element endplate. Endplate strips were either machined or stamped with the long dimension parallel to the "transverse" or "longitudinal" directions of the as-received parent endplate strip material. The longitudinal direction corresponds to the rolling direction of the strip. Five endcaps were welded to the endplate strip using standard production welding procedure. The test matrix encompassed differences in manufacturers (General Electric Canada and Zircatec Precision Industries Incorporated), orientations of the strips, loading frequency (0.1-20 Hz), temperature (room temperature and 310°C), and R-ratio (ratio of minimum load to maximum load for the cycle).

The design of the loading fixture is presented in Figure 3. Loads were applied to produce an axial displacement of the centre endcap with respect to the other four endcaps which were axially fixed. Under this loading condition, the two welds adjacent to the centre weld and the endplate strip at the centre endcap will be under bending stress. The two endcaps at the end of the specimen were not stressed. The main function of the 4.8 mm (3/16") diameter drill rods was to provide axial stiffness and lateral flexibility to simulate the behaviour of the outer ring fuel pencils when they are subjected to axial loading. Prior to carrying out cyclic tests, some tensile tests were performed at both room temperature and 310°C to obtain load vs ram displacement data.

The fatigue testing was carried out in a "load-control" mode in a servohydraulic MTS testing machine. The loading waveform used was a haversine and the cyclic stress was tension-tension. The 310°C tests were performed in a three-zone resistance furnace. In general, tests were carried out to specimen failure. For some of low frequency (≤ 1 Hz) tests, the load and ram displacement cycles were monitored using a chart recorder. The increase of the peak position of the ram with increasing cycles or test time gives an indication of the degree of fatigue crack growth in the weld specimens.

3.0 RESULTS & DISCUSSION

3.1 Analysis of Fatigue Specimen

Analysis is required to interpret the data obtained from the small specimen program for application to the reactor situation. A simple stress analysis of the sample in the loading jig was carried out using ABAQUS with "B23" cubic beam elements. Figure 4 illustrates schematically the models used for the analysis. The stresses reflect the net moment near the joint. No attempt was made to determine the detailed stresses at the weld but rather the nominal stresses in the endplate at the edge of the weld were calculated at a distance of 2.29 mm from the weld centre. This distance was chosen to be consistent with the manufacturer's stress analysis of the bundle.

Several cases were examined to determine the effects of modulus change, joint rigidity and jig rod length. Although calculated deflections were significantly altered in these cases, the stresses were not greatly affected (Table 1). Based upon this analysis, a factor of 1.3 MPa/N was used to convert applied loads to nominal stresses.

Table 1

Normalized Nominal Bending Stress (σ/P (MPa/N))
and Central Deflection (u/P)

CASE	h (mm)	σ/P in MPa/N at x (mm)				u/P (mm/N)	NOTES
		1.0	2.0	3.0	4.0		
1	76.2	1.64	1.38	1.12	0.86	1.13e-3	
2	76.2	1.64	1.38	1.12	0.86	1.13e-4	increase moduli 10x
3	76.2	1.65	1.39	1.13	0.87	5.82e-1	joints E = 0.1GPa
4	76.2	1.63	1.37	1.11	0.85	4.94e-4	joints E = 100000GPa
5	76.2	1.63	1.37	1.11	0.85	4.94e-4	MPC joints
6	25.4	1.68	1.42	1.15	0.89	1.07e-3	effect of rod length
7	50.8	1.66	1.40	1.14	0.88	1.10e-3	effect of rod length
1	76.2	1.64	1.38	1.12	0.86	1.13e-3	effect of rod length

3.2 Fatigue Life Data

3.2.1 Tensile Tests. The tensile load vs ram displacement data presented in Figure 5 have the general shape of a load vs elongation curve obtainable from a standard uniaxial tensile test. This shows that the specimen deformed initially in a elastic manner. With increasing applied load, the deformation of

the specimen became plastic and concentrated in the endplate in the immediate vicinity of the welds associated with the three central endcaps.

3.2.2 Fatigue Life Data. Two cracks are produced in each test. These are in the welds of the two endcaps adjacent to the centre endcap. The fatigue data are presented in the form of a log-log plot of applied stress amplitude vs cycles to failure (Figure 6). The applied stress amplitude was converted from applied load amplitude using the factor of 1.3 MPa/N obtained in Section 3.1. The data leads to the following observations:

(1) The fatigue curve for endplate-to-endcap welds lies significantly below the values available in the literature for smooth specimens. The line in Figure 6 represents the curve summarizing the results of O'Donnell and Langer(1). For the high cycle region at high R-ratio, the weld can sustain a stress amplitude which is only one quarter of that for a smooth specimen. In other words, the effective stress concentration factor of the weld notch is about four.

(2) There is a significant effect of mean stress on the minimum stress amplitude which produces failures in one million cycles. Higher mean loads can reduce the fatigue limit by a factor of about two in the range of tests conducted (Figure 7). Testing is continuing to construct a Haigh diagram to determine the effects of mean stress on fatigue life. For those tests carried out at high R-ratio, a stress amplitude of 45 MPa can produce failures between 10^5 and 10^6 cycles.

(3) Differences in fatigue life due to manufacturer, plate orientation and temperature appear to be small.

3.2.3 Crack Initiation & Propagation . Crack propagation behaviour for some tests was monitored with ram displacement. For a few selected tests, the cracking was monitored using potential drop measurement. The ram displacement technique effectively measures the change in compliance due to both cracks whereas the potential drop method monitors change in each crack individually. Figure 8 shows results of one test in which the crack growth was monitored using both techniques. Both types of measurements show that changes are occurring during the early part of the test that signify crack growth. The presence of the weld notch appears to remove the initiation stage as the life-determining step. The relatively small scatter in the experimentally determined lifetime (compared with usual fatigue data for smooth specimens) shown in Figure 6 is attributed to the presence of the notch.

A crack propagation analysis using fracture mechanics was carried out in order to determine whether the failure lifetime behaviour observed in the testing program could be rationalized with fatigue crack propagation data for Zicaloy reported in the literature(2). A simplified model was constructed in which crack

growth was assumed to start from a small semi-circular crack in a plate of infinite width. Crack growth was assumed to follow the Paris law:

$$da/dN = C\Delta K^n$$

The range of the stress intensity factor is:

$$\Delta K = \Delta \sigma f\sqrt{\pi a}$$

where

$\Delta \sigma$ = stress range

a = crack depth

f = a geometry correction factor

Literature data were used to calculate the fatigue crack growth rates. When the crack grew to the width of the test specimen, the model width was changed from infinity to the width of the experimental endplate strip and the crack front was assumed to be straight thus producing a 2-D model. Subsequent growth was also assumed to follow the same Paris law.

The comparison between the modelled lifetimes and measurements is shown in Figure 9. The effects of different assumptions of initial crack depth are shown in the Figure. The agreement between the model and the measurements is good considering the simplifying assumptions used. Figure 10 shows the inverse comparison, viz. fatigue crack growth rates implied by the lifetime measurements compared with data from the literature. Again, there is reasonable agreement.

The analysis also showed that a large fraction of the fatigue life is expended in the development of the crack to the width of the plate.

3.2.4 Formation of "Beach Marks". Beach marks were observed on some of the Darlington endplate cracks. Tests carried out to determine the necessary conditions for fatigue beach mark production showed that the key factor was the propagation of the crack at two or more different low stress amplitudes near the threshold level. A finite amount of crack propagation under each condition was found to be necessary in order to produce the marks. No beach marks could be produced either by varying the test frequency between 0.01 Hz and 20 Hz or by varying the test temperature at constant load amplitude. Beach marks were produced at both room temperature and at 310°C although those produced at 310°C were more visible.

3.3 Post Test Examination

Since the small specimen test program covered a large range of loading stresses, a selected group of the small specimen cracks were characterized to serve as a reference for comparison with the Darlington endplate cracks. Metallographic sections were prepared across the centre of the weld along the long direction of the strip. The fracture surfaces were examined in the stereomicroscope and scanning electron microscope (SEM).

3.3.1 Microstructure of Weld. Figure 11 shows the profile and microstructure of a GEC and a Zircatec weld. The microstructure of the resistance weld reflects the thermal history (peak temperature and cooling rate). The weld consists mostly of equiaxed prior beta grains containing an acicular plate-shaped alpha phase. The weld boundary consists of recrystallized fine alpha grains adjacent to the slightly elongated cold rolled base metal alpha grains. A discontinuous fissure is present at the periphery of the interface between the endplate and the endcap. Zircatec welds had a larger notch radius and a smaller weld size than the GE welds.

Microhardness survey (Figure 12) showed that the weld was significantly harder than the base metal. However the hardest region was found in the fine grain structure at the periphery of the weld interface.

3.3.2 Characterizing Fatigue Cracks. Post test examination showed that fatigue load affected specimen deformation, location of crack initiation and crack path, surface topography and fracture appearance. The observations are summarized below with an emphasis on the difference between high (>10,000 cycles) and low cycle fatigue failures.

Crack Initiation - Cracks were initiated from the notch at the periphery of the weld (Figure 13). The location of crack initiation extended further into the weld fissure and within the prior beta region when the fatigue stress was high. Multiple crack initiation produced the many ridges on the fracture surfaces. Ridge height increased with stress.

Crack Propagation - In high stress low cycle (<thousands of cycles) failure, the crack path was nearly perpendicular to the endplate surface and did not follow the weld profile. In low stress high cycle failures, the cracks tended to follow the weld profile and form a smaller angle with the endplate-to-endcap interface plane (Figure 13). This indicates that the crack path is sensitive to weld microstructure at low fatigue stress. Crack path was essentially transgranular.

Fracture Surface Roughness - The roughness of the fracture surface depended upon the loading conditions. Rougher fracture surfaces were observed when the upper load limit of the fatigue cycle exceeded the elastic limit (based on the tensile behavior shown in Figure 5). There were no observable difference in surface roughness between the ambient and elevated temperature tests when the maximum stress was below the yield stress at the respective test temperatures.

Beach Marks - Fracture surface features resembling fatigue "beach marks" can be produced by varying the load amplitude within the low stress regime (Figure 14). The beach marks were visible due to small differences in the amount of flat fracture features on the crack surface. Without changing the applied load amplitude, no beach marks could be produced either by varying the test frequency or the test temperature.

Fracture Appearance - Fracture surfaces of the high stress low cycle cracks displayed many ductile features and a large shear lip. As the number of cycles to failure increased, the fracture surface became more brittle-looking. Fatigue striations were not frequently clearly identified. They were more readily observed in the alpha grain region and were clearly visible in samples which failed in 44,000 cycles (Figure 15). With very high cycle failure, regions of crystallographic brittle fracture were present and no fatigue striations could be observed in the SEM (Figure 16).

Comparison With Field Failures - The Darlington endplate fatigue cracks on the outer ring had macroscopically "smooth" fracture surfaces, beach marks, fine fatigue striations and small shear lips. The cracks tended to follow the weld profile. These features are consistent with the low stress high cycle cracks observed in the small specimen program.

4.0 SUMMARY

This testing program has provided considerable insight into the behaviour of the endplate-to-endcap weld under bending fatigue loading conditions. The fatigue data together with the stress analysis suggest that there is a significant stress concentrating effect of the notch at the intersection of the endcap and the endplate. A nominal stress amplitude of 45 MPa combined with a high mean stress are sufficient to produce failure in less than one million cycles. These stress amplitudes are calculated on a basis consistent with the GEC stress analysis of the fuel bundle. Larger stress amplitudes are required to produce failure in the same number of cycles if the mean stress is reduced. Test results at room temperature and at 310°C are not very different.

The crack path and fracture surface features are dependent upon the loading conditions which produce the failure. The Darlington endplate cracks are consistent with the features of low stress high cycle fatigue cracks produced in the small specimen test program.

ACKNOWLEDGEMENTS

This work was funded by Darlington Engineering of Ontario Hydro. Mr. M. McGraw and D. Carpenter carried out the fatigue testing. Metallography and fractography were done by A. Donner and R. Jarochowicz respectively.

REFERENCES

- (1) W.J. O'Donnell and B.F. Langer, "Fatigue Design Basis for Zircaloy Components", Nuclear Science and Engineering, 20, 1 (1964).
- (2) Pickles, B.W. and Picker, C, SMIRT 6, Paris, France. Paper f6/4, 1981.

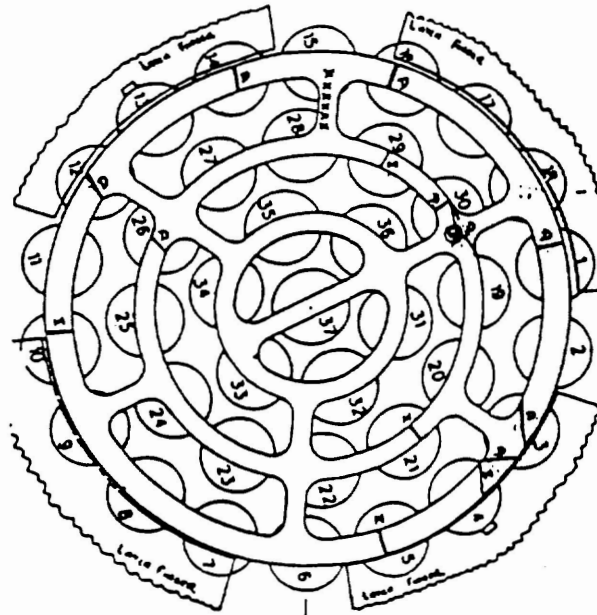
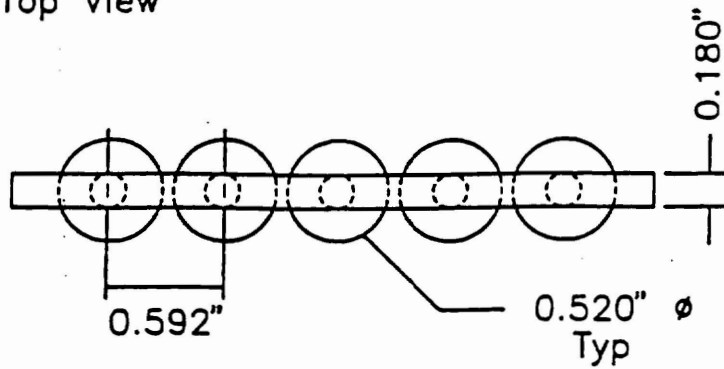


Figure 1. Schematic Diagram of Cracks Observed during Video Examination of Bundle 1 in Channel K12 of Darlington Unit 2.

Top View



Side View

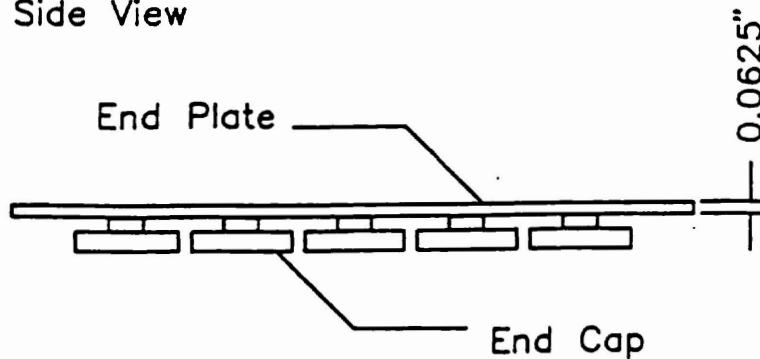


Figure 2. Schematic Diagram of the Endcap/endplate Weld Test Specimen.

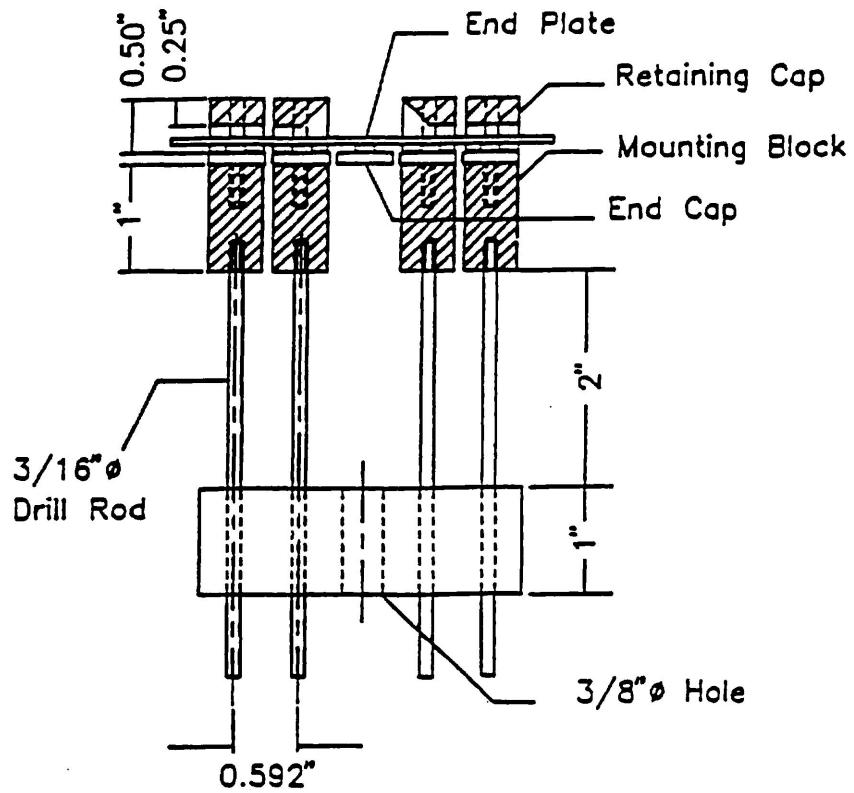


Figure 3. Schematic Diagram of the Loading Fixture developed for the Fatigue Testing of the Endcap/endplate Weld Specimens.

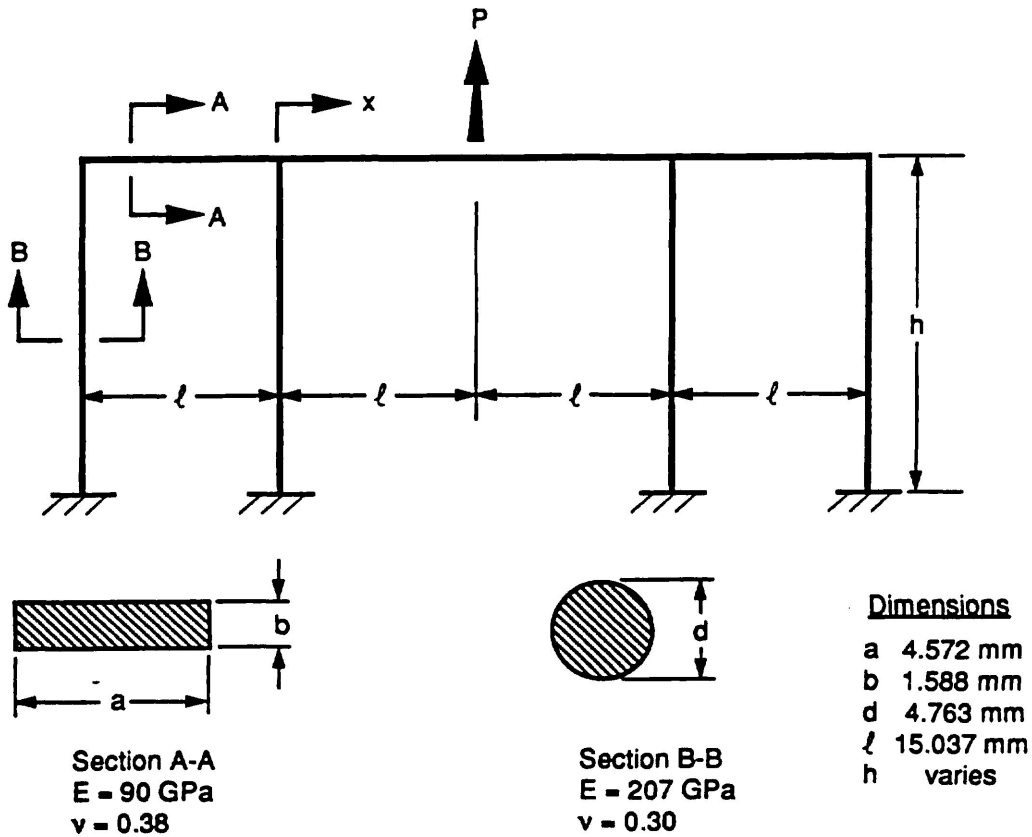


Figure 4. Finite Element Beam Model of Fatigue Specimen.

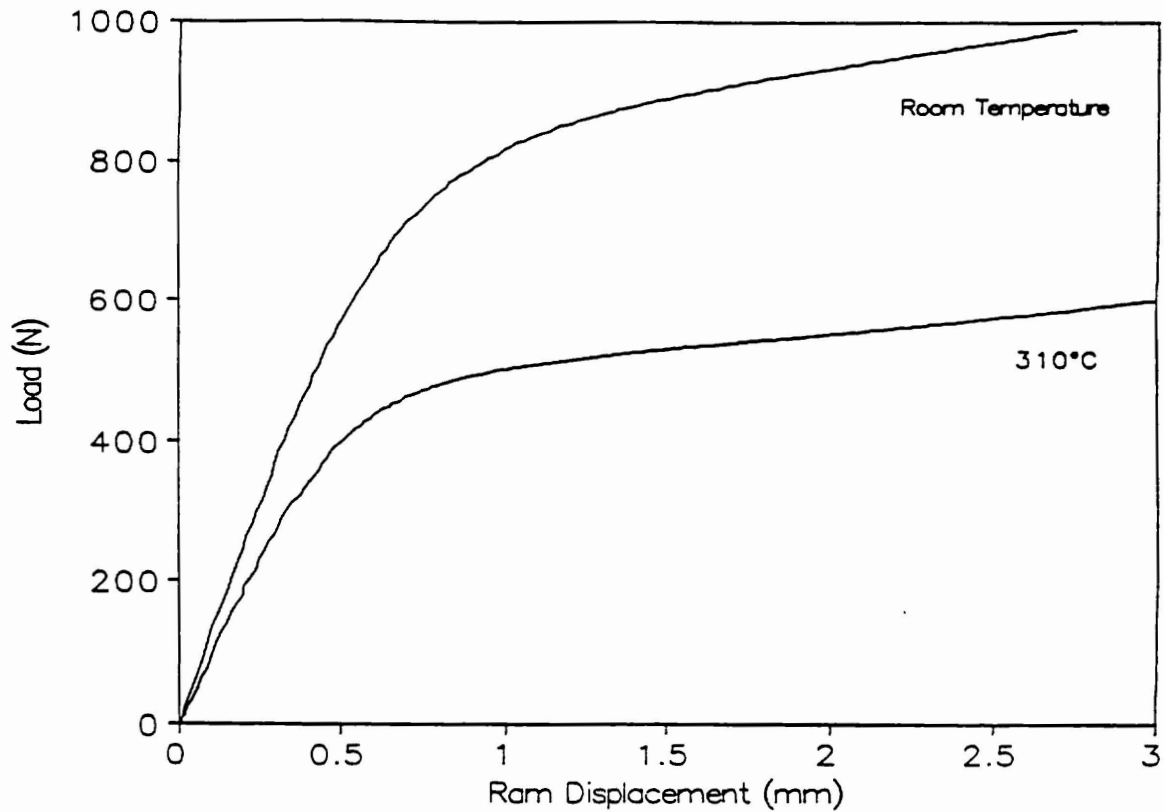


Figure 5. Experimental Load vs Ram Displacement Data for Tensile Tests carried out at Room Temperature and 310°C using GEC Transverse Endcap/endplate Weld Specimens.

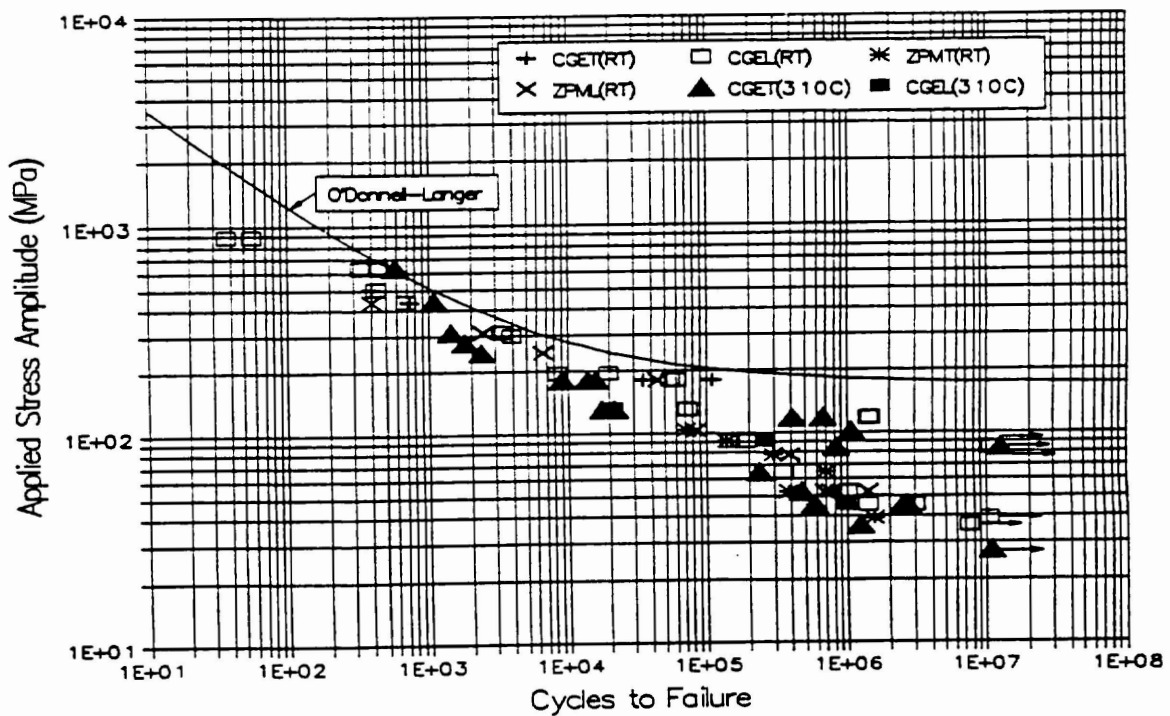


Figure 6. Effects of Applied Stress Amplitude on Fatigue Life of Endcap/endplate Weld Specimens.

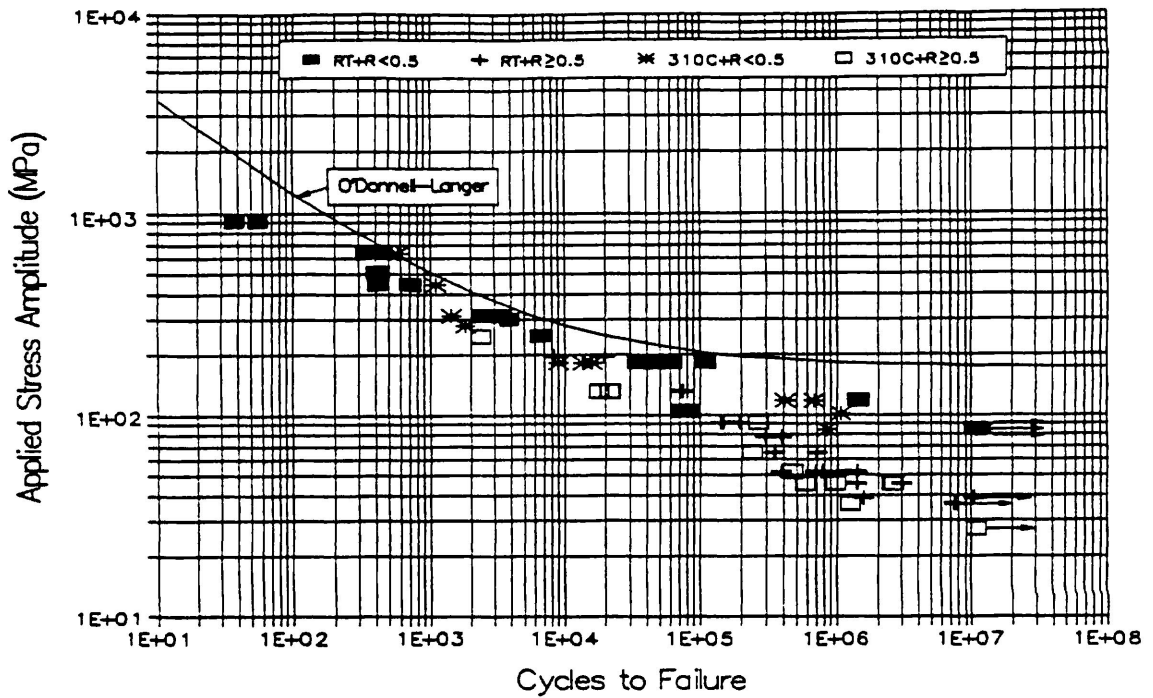


Figure 7 Same Data as Figure 6 but Showing the Effects of R-ratio on Fatigue Life.

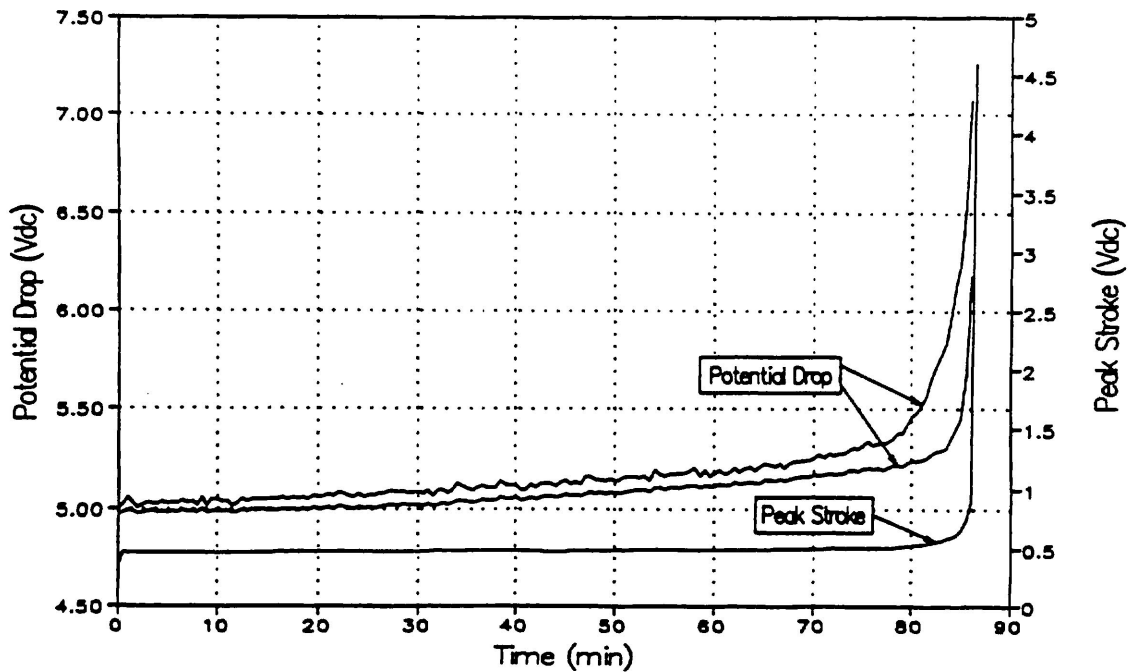


Figure 8. Increase in Ram Displacement and Potential Drop Across the Crack indicated that cracking occurred early on during Fatigue Testing.

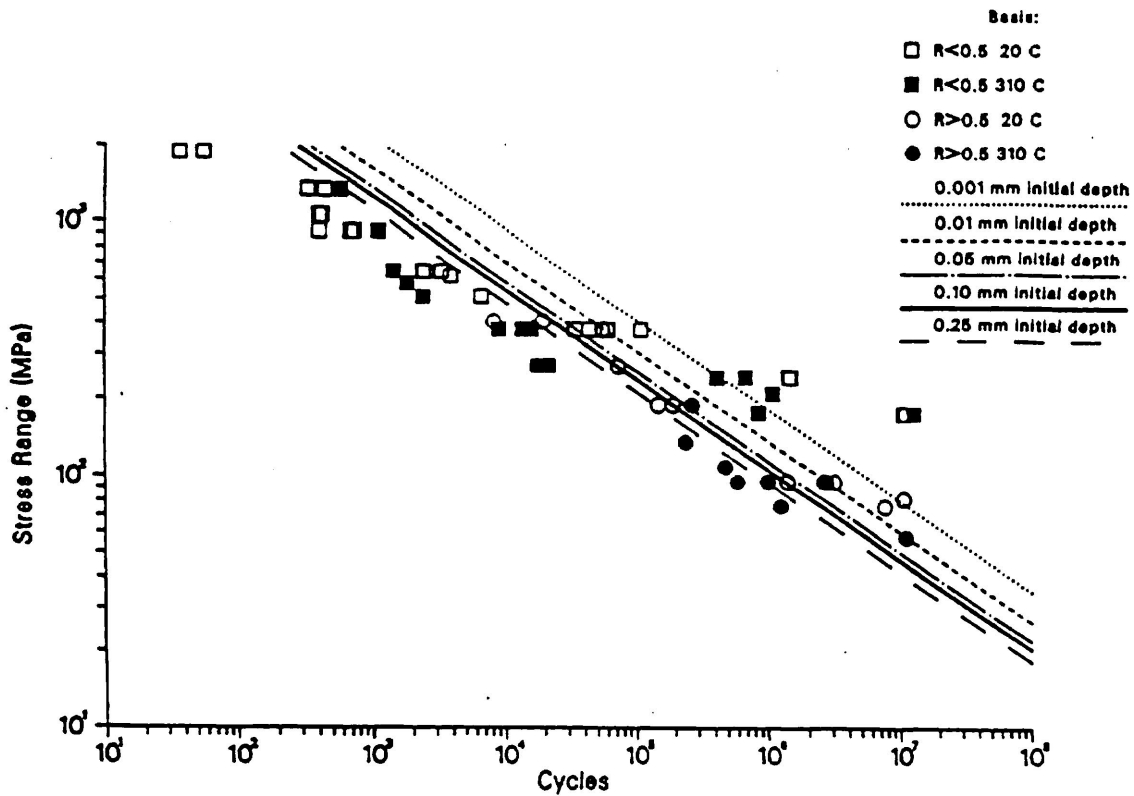


Figure 9. Comparison of Fatigue Test Results With Crack Growth Simulations (Effect of Assumed Initial Crack Depth).

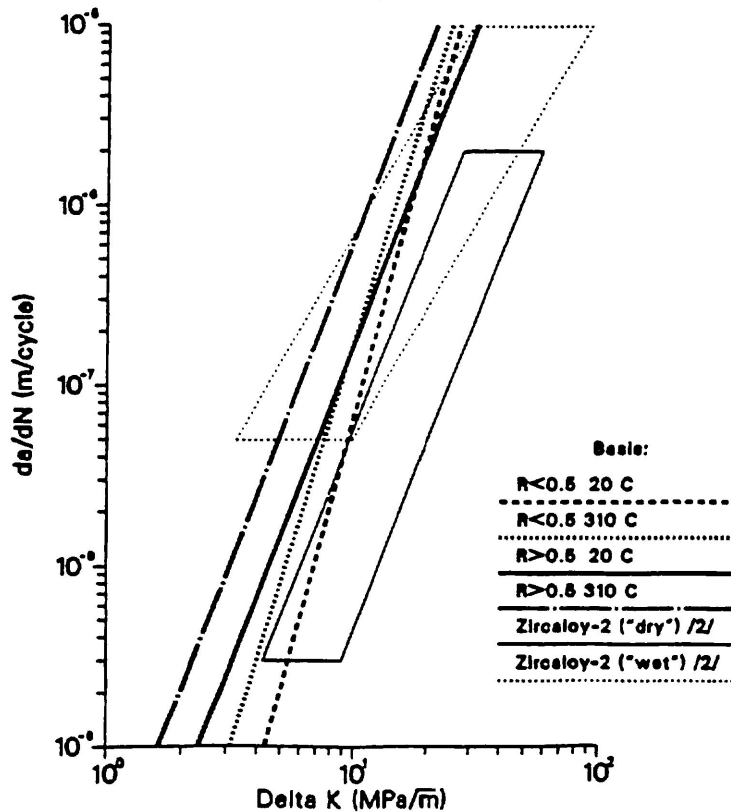


Figure 10. Comparison of Fatigue Crack Growth Data Implied by Small Specimen Program with Published Data.

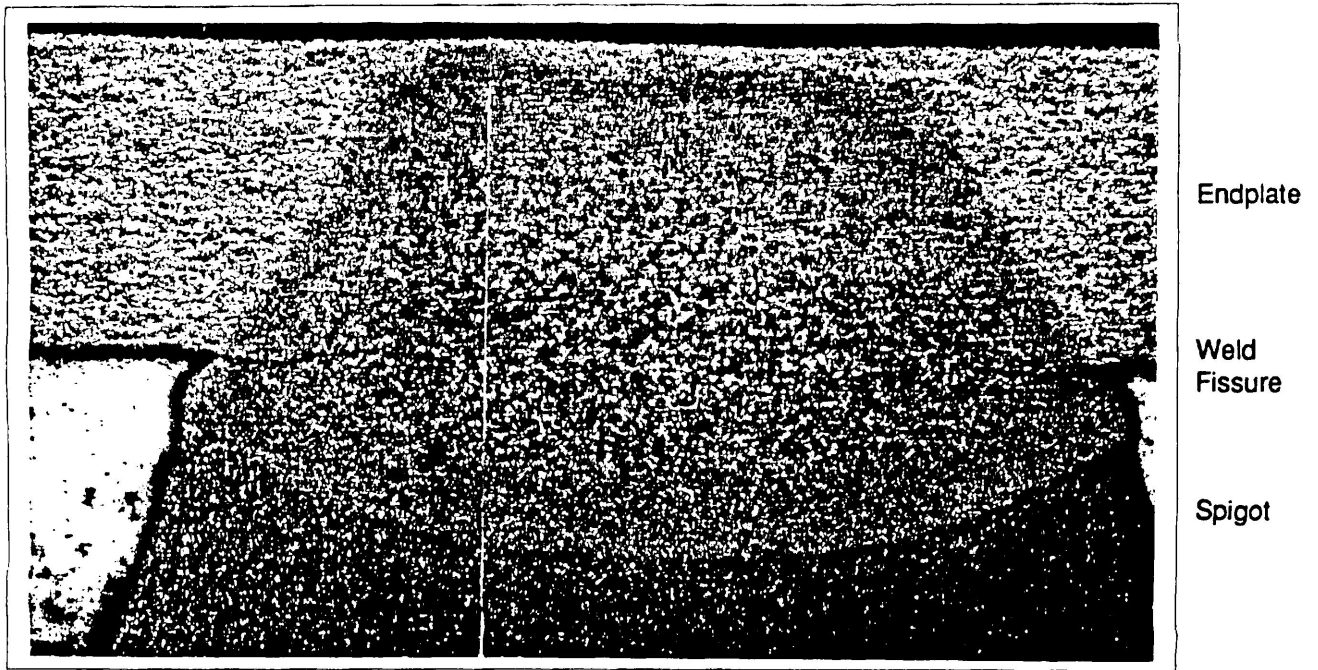


Figure 11. Microstructure and Profile of a GEC Endplate Weld. 25X.

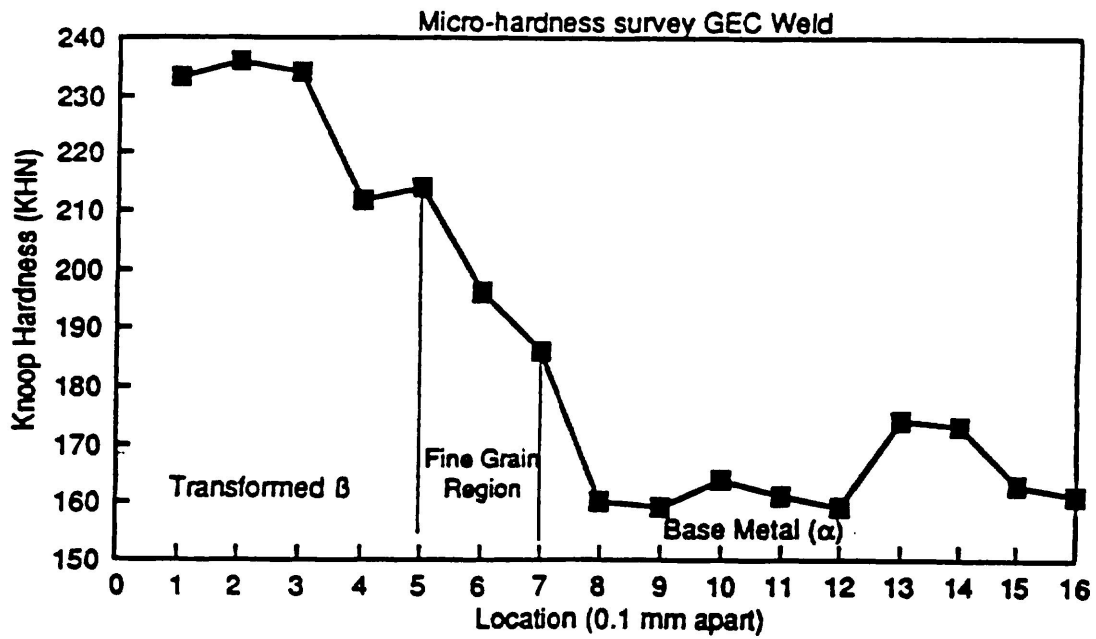


Figure 12. Micro-hardness Across the Weld Region of a GEC Endplate Weld.

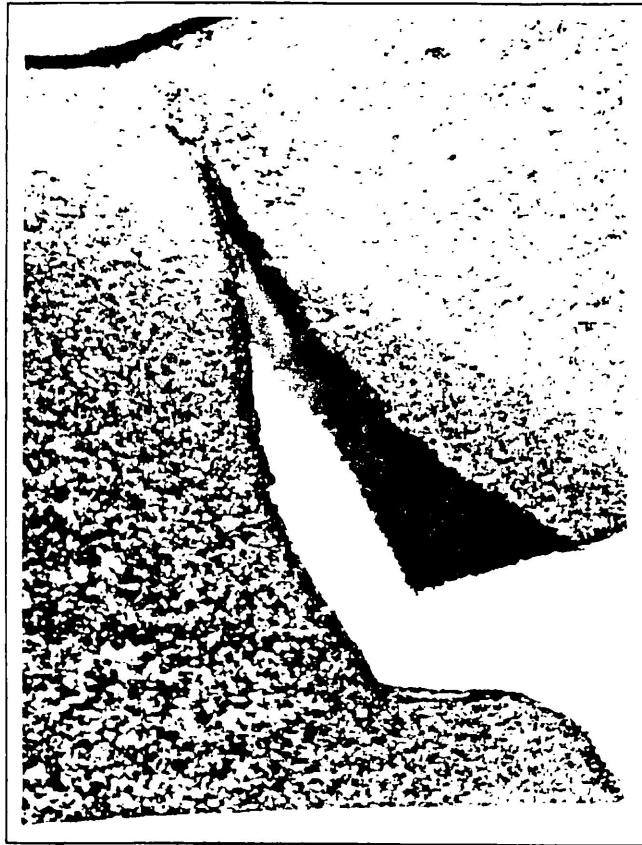


Figure 13a. This Specimen Failed in 728 Cycles at 20°C with Cyclic Stresses of 26 and 910 MPa. The Crack Initiated further into the Weld Fissure and the Crack Path did not follow the Weld Profile. 50X.

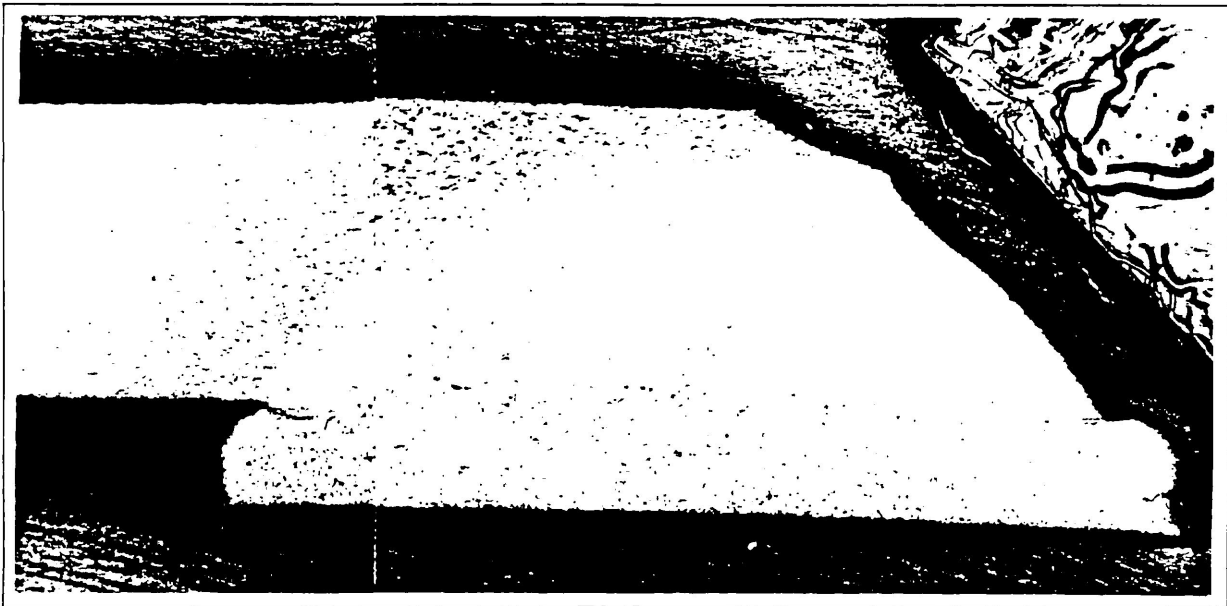


Figure 13b. This Specimen Failed in 1.4 Million Cycles at 20°C with Cyclic Stresses of 26 and 260 MPa. The Crack Initiated near the Weld Notch and Crack Path Follow the Weld Profile. 25X.

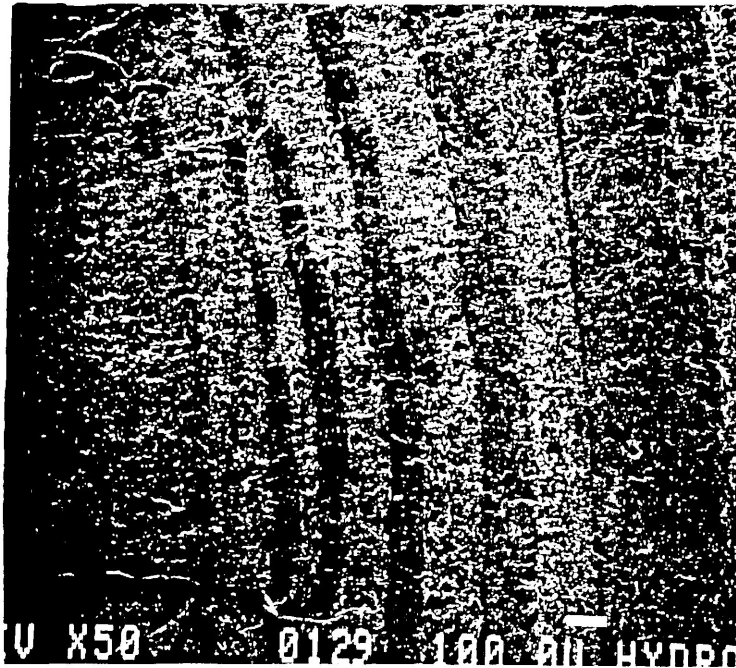


Figure 14. Beach Marks were formed on the Fracture Surface by Propagating the Crack at Different Stress Amplitudes near the Threshold Level.



Figure 15. Fatigue Striation in the α Grains Region in a Sample Failed in 44,000 cycles at 20°C.

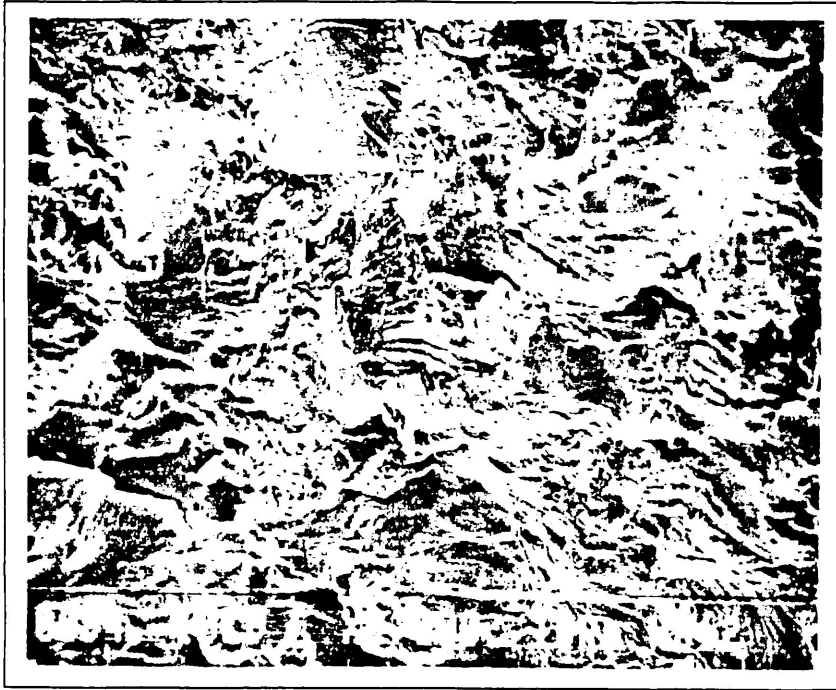


Figure 16. Faceted Crystallographic Fracture Appearance in a Sample Failed in 1.4 million cycles at 20°C. No Fatigue Striations could be Resolved in the SEM.

